



CSUG/SPE 138975

# Imaging Texture and Porosity in Mudstones and Shales: Comparison of Secondary and Ion-Milled Backscatter SEM Methods

M. Milner, R. McLin, J. Petriello, TerraTek



This paper was prepared for presentation at the Canadian Unconventional Resources & International Petroleum Conference held in Calgary, Alberta, Canada, 19–21 October 2010.



## Abstract

Observations from a number of unconventional reservoirs lead us to conclude that four major pore types exist in fine-grained reservoir and non-reservoir rocks, that they are effectively connected, and that pore sizes from nanometers to microns must be considered when evaluating size distributions. This paper uses SEM imaging of Haynesville, Horn River, Barnett and Marcellus Shales to illustrate that pore types other than those hosted by organics are present in unconventional shale gas reservoirs, and that they are continuous and connected to kerogen-hosted pores. In addition, we present evidence that the maximum size of pores originating in organic matter is determined by the size of the kerogen mass (in the case of organic particles) or the geometry of enclosing crystals (in the case of amorphous, pore-filling kerogen). Pairs of secondary and ion-milled backscatter SEM images address the misconception that large pores observed in secondary electron images are grain pullouts.

2-D image analysis and 3-D volumetric reconstructions to study pore distributions should take rock microtexture and the various pore types into consideration. A combined method using thin section textural analysis, XRD, and SEM imaging is recommended to address scaling issues when choosing samples for 2-D and 3-D volumetric analysis.

## Introduction

Petrologic and petrophysical work in a number of unconventional reservoirs leads us to conclusions similar to those of Schieber (2010), namely that a number of pore types exist in both reservoir and non-reservoir rocks, that they are effectively connected, and that pore sizes from nanometers to microns must be considered when evaluating size distributions. In this paper we confirm and illustrate the relative importance of pore type, size, and arrangement in examples from four North American gas reservoirs - Barnett Shale, Haynesville Shale, Horn River Shale, and Marcellus Shale - using combined secondary and ion-milled backscatter imaging.

Attention is given to lithotypes, matrix texture and composition and their influence on organic distribution and porosity. Whereas some previous work suggests that the organic material makes up most of the gas pore volume, and that gas calculation can be made considering only pores less than 1 micron (1000 nm) in size (Ambrose, et al., 2010), the work presented here supports a broader range of effective pore types and sizes, with evidence of probable conductivity between types. In addition we address the misconception that large pores observed in secondary electron images are grain pullouts (Loucks et al. 2009; Sondergeld et al. 2010). Ion-milled images suggest that the factors controlling maximum pore size are the size of the organic mass, or the geometry of the largest intercrystalline void (in the case of amorphous, pore-filling kerogen).

## Methods

Samples examined for this paper were cut from whole core collected from gas-productive reservoir rock of the Jurassic Haynesville Shale, Devonian Horn River Shale, Mississippian Barnett Shale, and Devonian Marcellus Shale. Two preparation techniques were used for SEM imaging. Secondary electron images represent fresh, minimally gold-coated surfaces broken normal to bedding. Backscatter images show milled surfaces approximately 1.0 mm by 0.5 mm, created using a JEOL IB-9010 Argon-ion polisher. Both secondary and milled backscatter samples were imaged using an FEI NovaNano 630 field emission scanning electron microscope. Identification of mineral components in both methods was confirmed using concurrent energy dispersive X-ray analysis (EDX), performed using an EDAX Genesis instrument.

XRD data were generated from powdered samples analyzed with a Rigaku Ultima III X-ray diffractometer, and results were interpreted using JADE software. Thin sections were cut to a standard thickness and stained with a mixture of potassium ferricyanide and Alizarin Red 'S' to aid in identification of carbonate minerals. Petrophysical measurements including porosity (% of bulk volume), gas-filled porosity and pressure-decay permeability to gas reported in this paper were produced using a modified GRI Method (Luffel et al. 1993; J. Keller, verbal communication). Geochemical measurements include weight percent total organic carbon (TOC) measured using industry standard procedure in a LECO EC-12 or LECO CS-444 carbon analyzer at about 1,000° C; and RockEval II pyrolysis. Ro values for Marcellus and Barnett samples are calculated from RockEval measurements (Jarvie, 2001), or in the case of Haynesville samples, vitrinite reflectance analysis was conducted in accordance with ASTM D 2798 specifications.

## Pore Types in Selected Unconventional Gas Reservoirs

Studies of numerous gas shale reservoirs suggest that matrix intercrystalline, organic, and intraparticle pores are the most common pore classes observed under scanning electron microscopy (SEM). Dissolution pores are found in all mudstones in minor amounts. Both secondary and ion-milled backscatter SEM images of fine-grained reservoir rocks allow examination of these pore types. *Matrix intercrystalline pores* are voids between clay flakes and aggregates, cement crystals, and larger detrital particles; *organic pores* range from tiny pores in kerogen masses to larger voids left by alteration of organic particles; *dissolution pores* result from diagenetic alteration of grains; and *intraparticle pores* form connected networks between nanofossil fragments coated with amorphous kerogen (primarily in fecal pellets). The first three of these are equivalent to phyllosilicate framework (PF) pores, organic matter (OM) pores, and carbonate dissolution (CD) pores described by Schieber (2010). To these we add a fourth class, intraparticle porosity, which is unique and volumetrically important in some reservoirs. Intraparticle porosity occurs as interconnected networks contained primarily in fecal pellets.

The three most common pore classes are identified in Figures 1, 2 and 3. We find the fourth class, dissolution pores, to be present only in minor amounts in the formations examined. SEM images of this pore type are well represented elsewhere (Schieber, 2010). Intergranular pores associated with grain-supported laminae in mudstones are not considered in this paper, but are significant contributors to mudstone and shale porosity where they occur.

*[Figures 1, 2, and 3: SEM images illustrating the four most common pore classes observed in gas reservoirs.]*

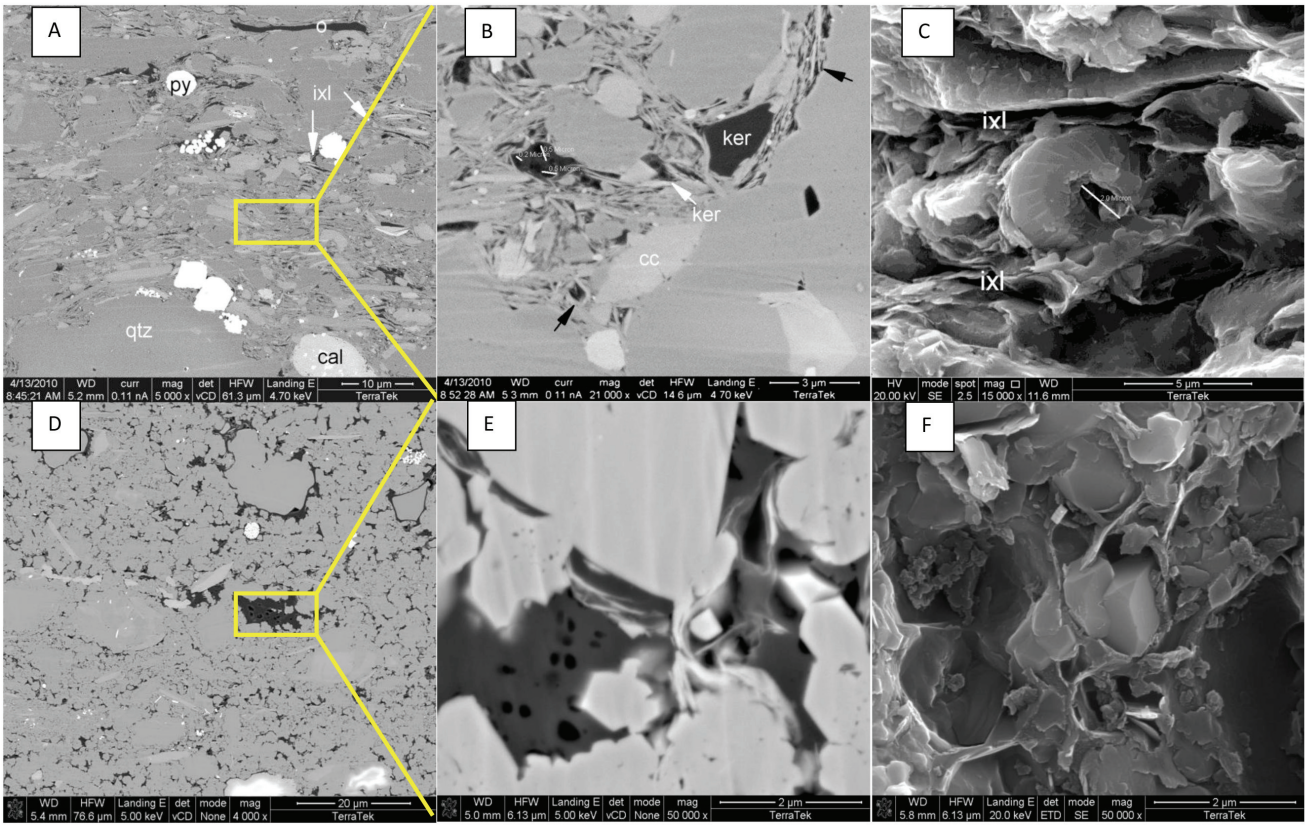


Figure 1: SEM images illustrating the two most common pore classes in unconventional gas reservoirs: matrix intercrystalline and kerogen-hosted organic pores. Top row, Haynesville Shale: (A) textural overview, silty calcareous/argillaceous mudstone. (B) Backscatter detail of pore system showing intercrystalline pores predominant (black arrows). (C) Secondary electron image at approximately the same scale as B. Flattened voids between clays (ixl) are interpreted as intercrystalline pores, as in B. Bottom row, Horn River Shale: (D) textural overview, siliceous mudstone. (E) Detail of D emphasizing organic porosity within kerogen mass. (F) Secondary electron image at the same scale showing rough, spongy kerogen morphology and organic pores.

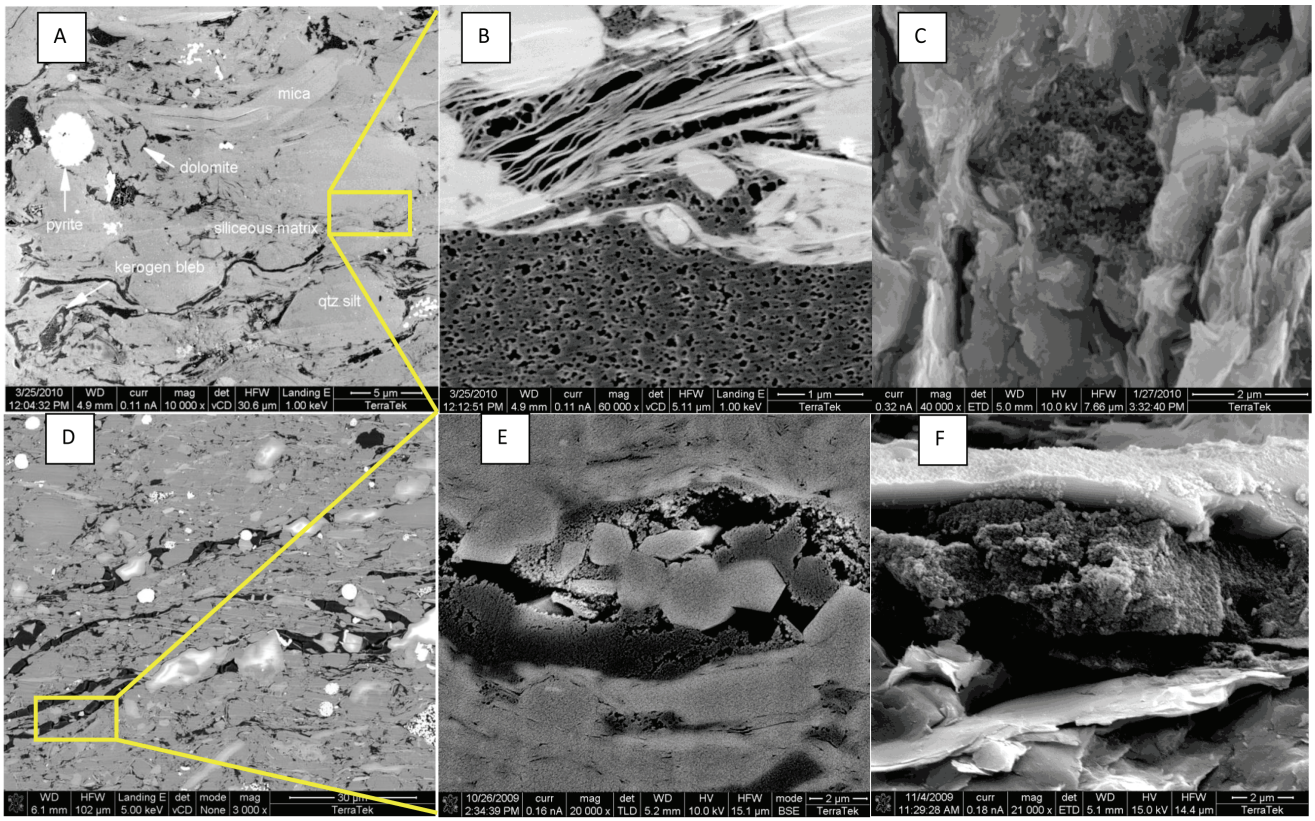


Figure 2: SEM images showing two types of organic porosity - pores associated with large particles or kerogen masses, another example of kerogen-hosted organic pores. Top row, Barnett Shale: (A) textural overview, siliceous mudstone, with textural elements labeled. (B) Enlarged view of kerogen-hosted (lower part of image) and intercrystalline (upper) pore types. (C) Secondary electron image at slightly lower magnification showing porous kerogen morphology. Bottom row, Marcellus Shale: (D) textural overview, argillaceous mudstone. (E) Backscatter detail of large altered organic particle and associated organic porosity. (F) Secondary electron image at approximately the same scale showing texture of the altered particle. The surrounding void is interpreted as an organic pore.

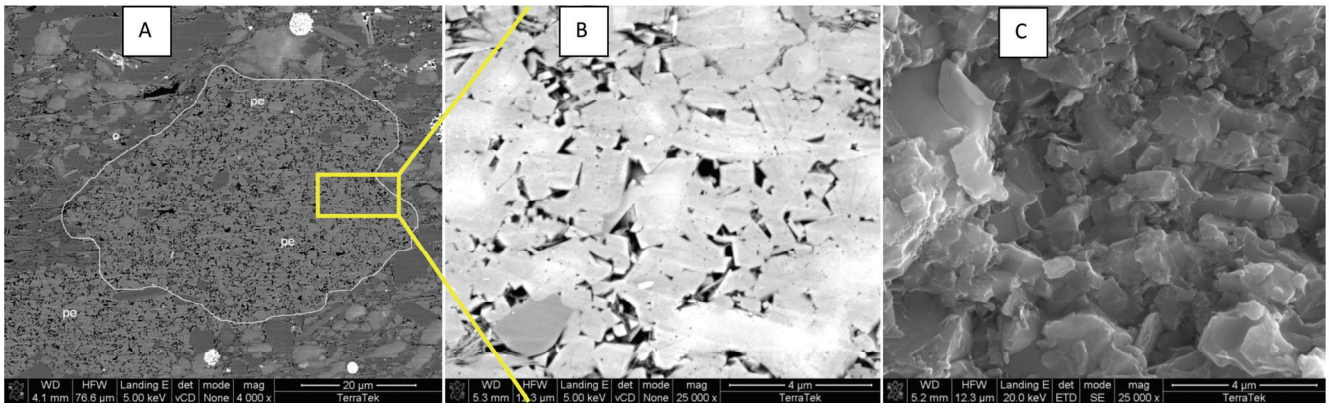


Figure 3: SEM images illustrating intraparticle pores. Haynesville Shale: (A) textural overview, calcareous/argillaceous mudstone. A calcareous fecal pellet is outlined (pe). (B) Enlarged view inside the fecal pellet. (C) Secondary electron image at the same scale showing filmy organics coating coccolith plates.

In rocks where intercrystalline pores are the predominant type, pore size and shape depends on the mineralogy, geometry and arrangement of adjacent particles. The Jurassic Haynesville Shale example in Figure 1 A, B and C illustrates a case where intercrystalline pores are dominant. Note that porous kerogen fills some voids (A and B, white arrows). Compaction, original grain structure, and depositional texture all play a role in determining this fine-scale arrangement of minerals; however, diagenetic overprints in both clays and other components supply a secondary control (see also Schieber, 2010).

In Figure 1 A quartz silt grains (qtz), calcareous particles (cal), pyrite framboids (py), and organic lenses (o) form wavy horizontally laminated microtexture slightly disturbed by bioturbation. Figure 1B is a backscatter detail of the pore system showing intercrystalline pores (black arrows) between illitic clay flakes, adjacent silt grains and calcite cement crystals. Ker = kerogen blebs, white arrow = intercrystalline pore with kerogen lining, cc = oblique view of a calcareous coccolith plate. Scale bars inside the kerogen mass at center left measure three organic pores as 0.2, 0.5 and 0.5 microns in size. Figure 1 C is a secondary electron image at approximately the same scale as B. In this case, the ion-milled backscatter image (B; black arrows) confirms that the flattened voids between clays (C; ixl) are intercrystalline pores rather than plucked grains (Loucks, 2009; Sondergeld et al. 2010). At center in image C is a coccolith wheel with a 2 micron diameter central cavity.

In contrast to the Haynesville sample, pores in a typical siliceous mudstone from the Devonian Horn River Shale (Figure 1, D through F) are mainly of the kerogen-hosted organic type. The matrix is composed of quartz grains and crystals of various sizes and minor clays, with a less laminated microtexture. Blocky, euhedral quartz crystals and isolated illitic clay flakes in E and F contrast with darker and spongy textured interstitial kerogen (Images E and F). Organic pores in kerogen masses (E) are less than one micron in size.

A siliceous mudstone from the Mississippian Barnett Shale (Figure 2 A, B and C) contains varied detrital and diagenetic particles (A). As in each row, the two leftmost images are ion-milled surfaces viewed under backscatter SEM. Gray-scale variations in backscatter images reflect contrasts in elemental atomic number (Z-contrast), making grayscale a proxy for mineralogy. Iron in pyrite or ferroan dolomite shows up as bright spots; clays, quartz cement and silt grains are lighter shades of gray similar in color. Organic matter has a low Z-contrast and appears as dark gray; calcite has a higher Z-contrast than illitic clays or quartz and appears lighter gray. Most porosity in the mudstone is of the kerogen-hosted organic type, although intercrystalline pores are also represented (pores between clays, top part of B). From these images, most organic pores measure in the tens of nanometers, whereas intercrystalline voids up to a micron are visible in B. Considering the close proximity of the two pore types, it seems reasonable to expect in a gas-charged system that both types contain gas. The secondary electron image (C) highlights the rough, spongy kerogen morphology, indicating gas-window thermal maturity.

Argillaceous mudstone of the Devonian Marcellus Shale is represented in Figure 2 D, E and F. Lenses and larger particles of organic matter (dark) align with bedding and define sub-millimeter scale lamination (LO type lamination; Core-Based Mudstone and Shale Classification: A Method for Petrologic Evaluation of Unconventional Gas Reservoirs, Milner et. al. 2010, in preparation). Alteration of these particles and masses provides an example of a larger subtype of organic pore. Images E and F, at approximately the same magnification, are details of large altered organic particles and associated organic pores. In parts of the Marcellus the maximum pore size is determined by the sizes of the kerogen masses or organic particles and the geometry of enclosing illitic clays and quartz crystals. Pores of this type up to ten microns in size have been observed. The light-colored crystals at center in E are authigenic quartz. The secondary electron image (F) shows the rough, granular morphology characteristic of thermally altered kerogen.

Figure 3 A, B and C show another calcareous/argillaceous mudstone from the Haynesville Shale, this one dominated by intraparticle porosity. The calcareous fecal pellet outlined in A is enlarged in B and C, and shows disarticulated coccolithophorid algae plates cemented in an interlocking framework. These pores, individually less than 1 micron in size, create an interconnected network with high effective porosity. Rectangular, biogenic calcite crystals in pellets (B) commonly exhibit films of amorphous kerogen. The secondary electron image at the same scale shows disarticulated coccolith plates extensively coated with nanoporous kerogen.

It is possible with these observations to make some general statements about pore types, their size ranges, and occurrences. Table 1 below summarizes observations from Figures 1 through 3. Compared with earlier studies of pore sizes (Nelson 2009; Wang et. al. 2009), images presented here show maximum sizes significantly larger than those interpreted for shales.

[Table 1]

| Pore Type | Characteristics | Size Range | Image Ref | Occurrence in Mudstones and Shales |
|---|---|---|---|---|
| matrix intercrystalline | voids between clay flakes, aggregates, cement crystals, and detrital particles | less than 1 micron to 5 microns | Fig1 A,B, C; Fig 2 B (top) | dominant in low TOC rocks and mature shales where organics are absent or converted |
| organic (kerogen-hosted) | tiny pores in kerogen masses | 10 nm to 2 micron | Fig 1 B, D, E, F; Fig 2 A, B (bottom), C | pervasive in moderate to high TOC systems with gas window maturity; rocks with finely disseminated, degraded algal kerogen; abundance increases with thermal maturity |
| organic (masses and particles) | larger voids left by alteration of organic particles | 50 nm to 10 microns | Fig 2 D, E, F | systems with particulate, lenticular or matty organic matter and gas window or higher maturity |
| intraparticle | connected networks between kerogen-coated fragments | 3 nm to 2 microns | Fig 3 A, B, C | common in facies with fecal pellets; concentrations of coccolithophorid algae |
| dissolution | voids left by mineral dissolution | 5 microns to 200 microns | not shown | grains, microfossils and pellets |
| intergranular | pores in grain-supported layers, not addressed in this paper | 10 to 200 microns | not shown | laminae in silty or sandy mudstones, and tight gas siltstones/sandstones; compacted burrows, bioturbated zones |

Table 1. Pore Types, Sizes and Characteristics as Observed from Selected Unconventional Gas Reservoirs

## Rock Microtexture Considerations

The SEM images in Figures 1 through 3 illustrate the relationship between sub-millimeter scale texture and porosity. Due to the extremely small sample size in SEM work (generally less than 0.5 mm), sampling and correct representation of larger areas are critical when upscaling results (Sondergeld et. al. 2010). A classification of sub-millimeter scale texture using thin sections is a logical next step. Figures 4 and 5 present thin section and backscatter SEM pairs representing common reservoir lithotypes in the same formations examined above.

[Figures 4 and 5]

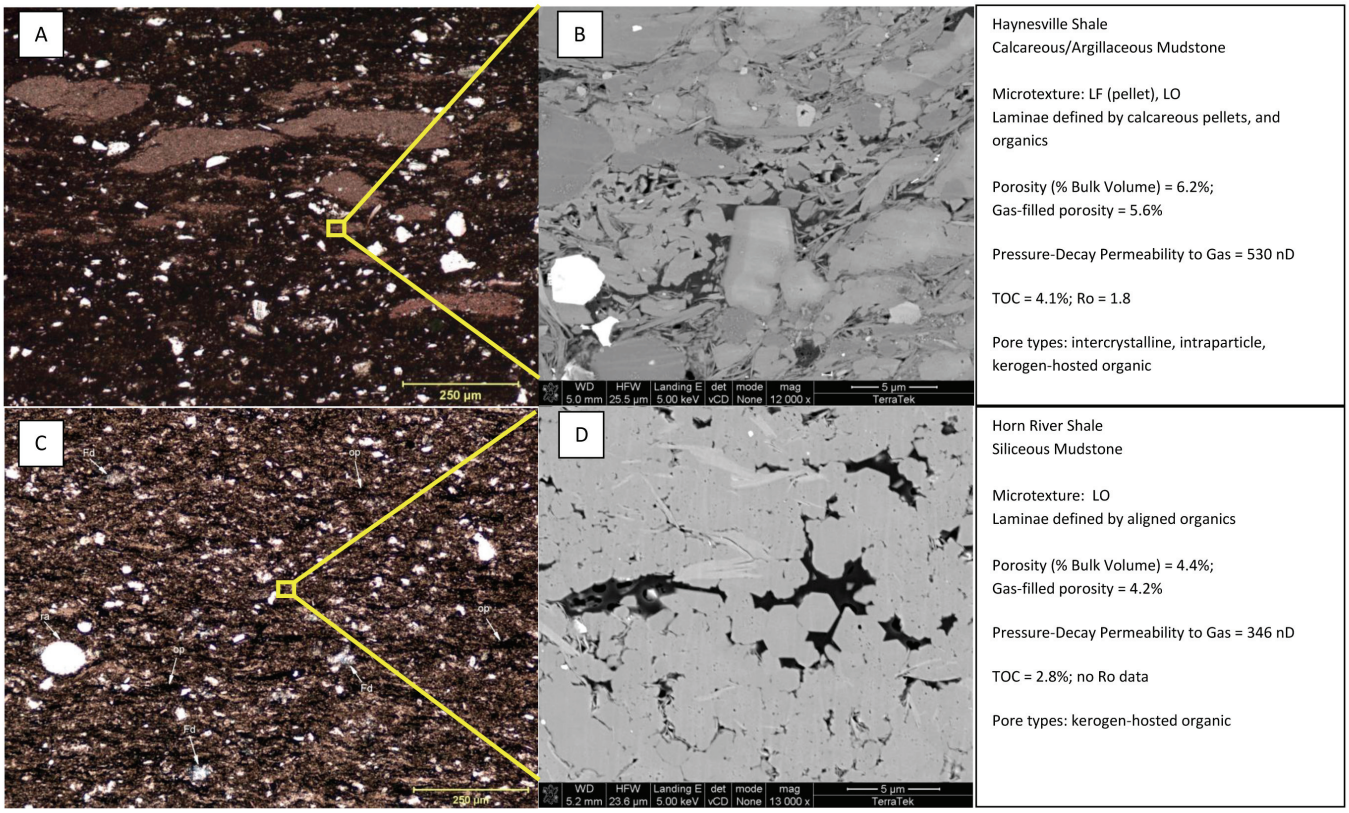


Figure 4: Sub-millimeter scale rock texture in typical reservoir lithotypes. Thin sections (left) reveal sub-millimeter scale lamination. Yellow rectangles approximate the size of area shown in SEM images (right). Low magnification ion-milled images show texture and distribution of organic matter and open pores, represented by darkest gray and black areas. (A) and (B), Haynesville Shale, silty calcareous/argillaceous mudstone; laminae are defined by compacted pellets and other fossils (LF), and to a lesser extent by organic layers. (C) and (D), Horn River Shale, siliceous mudstone. Sub-millimeter scale laminae are defined by bedding parallel lenses of organic matter (LO).

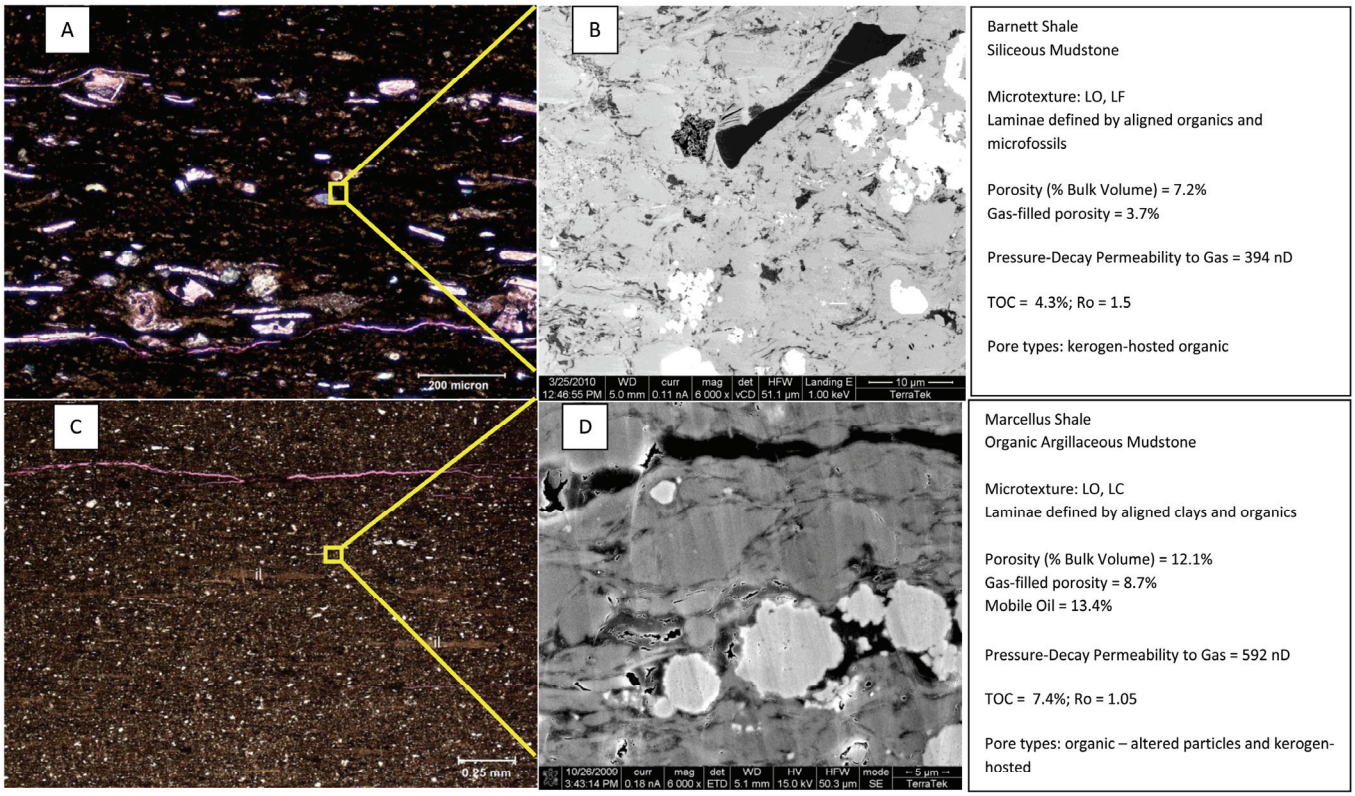


Figure 5: Sub-millimeter scale rock texture in typical reservoir lithotypes, continued. Thin sections (left) and Low magnification ion-milled SEM images (right). (A) and (B), Barnett Shale, siliceous mudstone; laminae are defined by layered organics (LO) and to a lesser extent by compacted calcareous and siliceous microfossils. (C) and (D), Marcellus Shale, argillaceous shale. Millimeter scale laminae are defined by variations in organic concentration (LO) and aligned illitic pods (LC). Chunks of organic matter up to 20 microns in length host relatively large organic pores. A number of elongate, intercrystalline pores are also visible between clay packets.

Each of the thin sections from the Haynesville (Figure 4 A), Horn River Shale (Figure 4 C), Barnett Shale (Figure 5 A) and Marcellus Shale (Figure 5 C) exhibit textures dependent on mineral composition, grain size, and organic matter. These microtextures are described in the panels at right of the respective images, along with a two-letter abbreviation for data collection purposes (Core-Based Mudstone and Shale Classification: A Method for Petrologic Evaluation of Unconventional Gas Reservoirs, Milner et. al. 2010, in preparation). Wide variations in texture at thin section scale, mostly related to lamination styles, make careful selection of SEM samples important in order to assure the best fabric representation. Thin sections provide a method of selection as well as a context for interpretation of SEM images.

Sub-millimeter scale textural details, when combined with petrophysical and other data (panels to the right of each pair) provide useful insights into how gas reservoir rocks behave and produce. Key observations from the sample set presented here are as follows.

- Figure 4 A and B: thin laminae composed of anastomosing pellets (stained pink in A) form surfaces of connected microporosity in certain pellet-rich lithotypes.
- Figure 4 C and D: nanoporous kerogen distributed in siliceous matrix forms a horizontal to almost boxwork network of connected micropores.
- Figure 5 A and B: organic matter in Barnett siliceous mudstone is highly dispersed and intimately associated with matrix authigenic quartz. However, unlike the Horn River sample, the mineral composition is more variable, with larger grain size and thus a secondary pore network of matrix intercrystalline pores.
- Figure 5 C and D: texture in Marcellus organic argillaceous mudstone is more strongly influenced by aligned clay fabric than other reservoir lithotypes. The Marcellus samples contain organic matter in larger lenses and particles than other reservoir rocks, and thus have potentially larger pore sizes in thermally mature facies (up to 10 microns).

- In general, lithotypes dominated by matrix intercrystalline pores or larger pores left by organic masses, have higher porosity and permeability values (i.e., Haynesville and Marcellus Shales).

**Relative Importance of Pore Types**

Secondary and backscatter SEM images indicate that matrix intercrystalline porosity, defined as voids between clay flakes and aggregates, cement crystals and larger detrital particles, is the ubiquitous pore type in mudstones and shales. Where organic porosity is highest (as in the reservoir lithotypes chosen for this paper), kerogen occupies these voids, as well as forming lenses, stringers, and particles. The greatest amount of open matrix intercrystalline porosity is present where total organic carbon is low, where minimally compacted matrix contains finely disseminated grain-coating kerogen, or where thermal maturation has converted most of the kerogen leaving open voids (organic pores).

A qualitative assessment of the relative abundances of pore types in the four shale gas formations is offered in Table 2 below. Such an assessment is necessarily subjective and is biased by the availability of reservoir rocks. However, based on many more than the few images presented in this paper, it is our opinion that these relative abundances apply in general to the main reservoir lithotypes for the four gas reservoirs listed. In Table 2, pore types are ranked 1 through 4, from most to least abundant as observed in SEM images.

It should be recognized that changes in the thermal maturity, texture, or mineralogy of the rocks will alter the observed ranking. Thus, the table is a generalization with many exceptions. As always, it is critical to make appropriate observations on the reservoir rock to be assessed.

[Table 2]

| | Formation | Haynesville | Horn River | Barnett | Marcellus |
|---|---|---|---|---|---|
| | Dominant Reservoir Lithotype | calcareous/argillaceous mudstone | siliceous mudstone | siliceous/argillaceous mudstone | argillaceous mudstone |
| Pore Type Rank | matrix intercrystalline | 1 | 2 | 2 | 3 |
| | organic (kerogen-hosted) | 3 | 1 | 1 | 2 |
| | organic (masses and particles) | ~ | ~ | 4 | 1 |
| | intraparticle | 2 | ~ | ~ | ~ |
| | dissolution | minor | minor | minor | minor |
| | intergranular | 4 | ~ | ~ | 4 |

Table 2: Relative Abundance of Pore Classes in Selected Gas Reservoirs.

Table 2: Relative Abundance of Pore Classes in Selected Gas Reservoirs. Pore types are ranked by relative abundance in the main reservoir lithotype named for the four formations compared. 1 = most abundant, 4 = least abundant, ~ = not observed.

**Conclusions**

Four major pore types are imaged in four well-known and productive unconventional gas shales via secondary and ion-milled backscatter SEM. Several pore types occur in close proximity or overlap in type, and therefore can reasonably be assumed to be connected. The Haynesville, Horn River, Barnett and Marcellus Shales show pore sizes ranging from nanometers to microns in size depending on matrix microtexture, grain size, mineralogy, organic type and thermal maturity.

If observed pore sizes are up to 10 microns and the various pore types are connected, 2-D and 3-D models of shale porosity based on focused ion beam (FIB) SEM cubes with dimension from less than 1 micron to 5 microns (Sondergeld et. al. 2010, Ambrose et. al. 2010) may not capture and represent all porosity in the rocks. 2-D image

analysis and 3-D volumetric reconstructions to study pore distributions should take rock microtexture and the various pore types into consideration. A combined method using thin section textural analysis and SEM imaging is recommended to address scaling issues when choosing samples for volumetric analysis.

Secondary electron imaging of broken samples allows assessment of particle and crystal shapes in 3 dimensions, and provides evidence of the condition (maturity) of organic matter. While pores are visible in broken samples, quantification of size and type is problematic, and intercrystalline pores can be difficult to distinguish from artifacts. The polished surfaces in ion-milled backscatter SEM allow better pore characterization and introduce the possibility of image analysis for quantification, if sampling and scale obstacles can be overcome.

**Acknowledgements**

The authors recognize William Zagorski and Martin Emery of Range Resources, David Spain of BP America, and Ann Cochran of Encana Canada for permission to publish the images and data presented here, as well as for their continued input to discussions. Thanks are due to TerraTek-Schlumberger for supporting this work, and to Kelly Vaughn, John Keller, Dave Handwerger, Tim Sodergren, and our many other colleagues for their ideas and insights.

**References**

ASTM Standard D2798-09a. Standard Test Method for Microscopial Determination of the Vitrinite Reflectance of Coal. ASTM International, West Conshohocken, PA, 2009. DOI: 10.1520/D2798-09. www.astm.org.

Ambrose , R.J., R. C. Hartman, M. Diaz-Campos, Y. Akkutlu, and C. H. Sondergeld, 2010. New Pore-Scale Considerations for Shale Gas in Place Calculations. SPE 131772, Unconventional Gas Conf., Feb-23-25, Pittsburgh, Pennsylvania, USA.

Jarvie, D. M., B. L. Claxton, F. Henk, and J. T. Breyer, 2001. Oil and shale gas from the Barnett Shale, Fort Worth Basin, Texas. AAPG Annual meeting Program, v. 10, p. A100.

Keller, J. Verbal Communication, 28 February, 2010.

Loucks, R. G., R. M. Reed, S. C. Ruppel, and D. M. Jarvie, 2009. Morphology, Genesis and Distribution of Nanometer-Scale Pores in Siliceous Mudstones of the Mississippian Barnett Shale. Journal of Sedimentary Research 79: 848-861.

Luffel, D.L., C. W. Hopkins, P. D. Schettler, 1993. Matrix Permeability Measurements of Gas Productive Shales. SPE 26633., 68th Annual Technical Conf. and Exhibition of the SPE, Houston, Texas, USA.

Milner, M., P. N. Gathogo, and B. Marin, 2010. Core-Based Mudstone and Shale Classification: A Method for Petrologic Evaluation of Unconventional Gas Reservoirs, in preparation.

Nelson, P. H., 2009. Pore-throat sizes in sandstones, tight sandstones, and shales. AAPG Bulletin, V.93, No. 3: 329-340.

Schieber, J., 2010. Common Themes in the Formation and Preservation of Intrinsic Porosity in Shales and Mudstones - Illustrated With Examples Across the Phanerozoic. SPE 132370, Unconventional Gas Conf., Feb-23-25, Pittsburgh, Pennsylvania, USA.

Sondergeld, C.H.,R.J. Ambrose, C.S. Rai, 2010. Micro-Structural Studies of Gas Shale. SPE 131771, Unconventional Gas Conf., Feb-23-25, Pittsburgh, Pennsylvania, USA.

Wang, F. P. and R. M. Reed, 2009. Pore Networks and Fluid Flow in Gas Shales. SPE 124253, SPE Annual Technical Conf. and Exhibition, Oct. 4-7, New Orleans, LA, USA.